The role of post-treatment of an ecofriendly cerium nanostructure Conversion coating by green corrosion inhibitor on the adhesion and corrosion protection properties of the epoxy c...

Article *in* Progress in Organic Coatings · January 2018

DOI: 10.1016/j.porgcoat.2017.09.015

CITATIONS
24

READS
322

3 authors, including:

Zeynab Mahidashti
Amirkabir University of Technology
10 PUBLICATIONS **84** CITATIONS

SEE PROFILE

B. Ramezanzadeh
Institute for Color Science and Technology
130 PUBLICATIONS **3,776** CITATIONS

SEE PROFILE

Progress in Organic Coatings 114 (2018) 19–32

Contents lists available at ScienceDirect

Progress in Organic Coatings

journal homepage: www.elsevier.com/locate/porgcoat

The role of post-treatment of an ecofriendly cerium nanostructure Conversion coating by green corrosion inhibitor on the adhesion and corrosion protection properties of the epoxy coating

Z. Mahidashti[a,*], T. Shahrabi[a,*], B. Ramezanzadeh[b,**]

[a] Department of Materials Engineering, Faculty of Engineering, Tarbiat Modares University, P.O. Box: 14115-143, Tehran, Iran
[b] Department of Surface Coatings and Corrosion, Institute for Color Science and Technology (ICST), PO 16765-654, Tehran, Iran

ARTICLE INFO

Keywords:
Nanostructure coating
Corrosion resistance
Adhesion
Green corrosion inhibitors

ABSTRACT

This study introduces a green strategy for enhancement of the corrosion protection and adhesion properties of an epoxy coating applied on the steel surface treated by cerium conversion coating (CeCC) and then post-treated by Urtica inhibitor. The corrosion behavior of the coatings was evaluated by electrochemical impedance spectroscopy and salt spray test. Scanning electron microscopy, energy dispersive spectroscopy, atomic force microscopy and contact angle measurements were adopted for surface characterization. For further investigations, pull-off and cathodic disbondment tests were performed. Results demonstrate the beneficial role of the post-treatment of CeCC by Urtica inhibitor on the enhancement of the epoxy coating performance.

1. Introduction

The use of organic coatings is considered as an effective method for the steel structures protection against corrosion in atmospheric environments. Durability and life time of an organic coating depends on several factors such as the coating chemistry, the density of the coating cross-links and adhesion to the metal surface. Among various coatings, epoxy coating, because of the high cross-linking density and good adhesion to the metal surface, has been considered for wide applications. However, diffusion of corrosive species into the epoxy coating from the inherent pores or scratches and access of these agents to the metal/coating interface result in the initiation of corrosion reactions at the anodic and cathodic sites [1]. The adhesion loss and coating disbondment as a result of pH rise on the cathodic areas and formation of corrosion products leads to the deterioration of the coating in the long term [2]. In this regard, one way to increase the corrosion protection properties of the epoxy coating applied on the metal surface is to improve its adhesion to the sub-layer. In recent years, various approaches such as alkaline and acid cleaning, mechanical preparation and chemical treatment by conversion and silane coatings have been considered by the researchers [3–6]. The pre-treatment of steel surface by conversion coating has been considered for decades in many industries. Conversion coating can be considered as a barrier against corrosive environments, limiting the access of water and corrosive ions to the substrate [7]. On the other hand, due to its semi-nonconductor entity, a conversion layer limits the electron transfer between the cathodic and anodic areas and in this way diminishes the corrosion rate on the metal surface, resulting in less adhesion loss of the epoxy coating in corrosive environments [8]. In addition, conversion coating has a porous structure, which increases the mechanical inter-locking and physical bonds between the diffused epoxy coating and the conversion layer, therefore enhances the dry adhesion of the epoxy coating [9]. It can also block the pores and channels of the epoxy coating and hinder the access of corrosive electrolyte to the active sites of steel surface [10]. In the case of metals with more than one oxidation state, such as chrome and cerium, a self-healing behavior can also be observed [11]. Chromate conversion coating is one of the widely applied chemical treatments for metal surfaces [12–14]. However, due to the presence of hazardous Cr (VI) species in the structure of this coating, the environmental legislations have banned its usage in recent years. Nowadays, more environmentally acceptable coatings, such as phosphate [15,16], zirconium [17,18], molybdate [19] and rare earth metal salts [20–22] have been developed and improved by different methods in order to replace the chromate chemical treatment and to provide reasonable corrosion protection of steel. Hamlaoui et al. [23] investigated a Cr-free layer based on Molybdate-phosphate-silicate (MPS) on galvanized steel. On the basis of EIS results, they revealed better electrochemical stability of MPS than chrome-containing layer in concentrated NaCl solution. Thus

* Corresponding authors.
** Co-corresponding author.
E-mail addresses: tshahrabi34@Modares.ac.ir (T. Shahrabi), ramezanzadeh-bh@icrc.ac.ir, ramezanzadeh@aut.ac.ir (B. Ramezanzadeh).

http://dx.doi.org/10.1016/j.porgcoat.2017.09.015
Received 19 July 2017; Received in revised form 23 August 2017; Accepted 28 September 2017
Available online 07 October 2017

it could be a promising alternative to chromate coating. Su et al. [24] showed that inclusion of Ni^{2+} and Mn^{2+} cations into the phosphate bath resulted in the decrease of coating porosity and grain size and thereby its corrosion resistance can be noticeably improved. Gang et al. [25] examined the corrosion behavior of lanthanum-based conversion coating modified with citric acid. Their results showed that the La conversion coating inhibited both cathodic and anodic reactions and provided a desirable barrier film against aggressive species diffusion toward the steel surface. Ghanbari et al. [26] revealed the enhanced adhesion properties of epoxy coating to the steel substrate through chemical treatment by zirconium-based conversion coatings. The improved performance was attributed to the increase of surface roughness and polar entity of the surface. Accordingly, the rare earth based conversion coating is another effective and environmentally friendly candidate for replacing toxic chromate conversion coating [27,28]. Cerium [29,30], lanthanum [31,32], praseodymium [33,34] and neodymium [35,36] are some important examples of rare earth compounds which have been used for surface treatment of various metals.

In recent years, many studies have focused on the application of this kind of coating on different metal surfaces [10,37,38]. However, problems such as cracking of the conversion layer and poor adhesion to the sub-layer are still a matter of challenge. Observations show that adding H_2O_2 as an accelerator to the cerium conversion bath increases the reaction rate but evolution of the resultant H_2 gas leads to the blistering and eventually adhesion loss of the coating from the substrate [39,40]. Furthermore, the cerium film experiences some additional cracks during drying stage, which is a result of stress release caused by water egression from the coating [41]. Hence, finding procedures for improving the corrosion resistance of the coating, especially through eliminating the structural cracks and therefore enhancing the adhesion properties of the applied epoxy coating is of great importance.

Hassannejad et al. [42] revealed the beneficial role of nanostructured cerium oxide conversion coating modified with chitosan on the AA2024 aluminum alloy corrosion resistance improvement. Lei et al. [43] reported the effect of silane agent on the microstructure and electrochemical behavior of cerium conversion coating on magnesium substrates. Loperena et al. [44] showed that addition of ascorbic acid as additive affects the microstructure and anticorrosive properties of the formed films. Yoganandan et al. [45] reported the Evaluation of corrosion resistance and self-healing behavior of zirconium–cerium conversion coating developed on AA2024 alloy. There are also many reports attempting to improve the adhesion properties of organic paints on metal surface via cerium based conversion coatings. Van Phuong et al. [46] showed that the adhesion and corrosion resistance of electrophoretic paint on AZ31 Mg alloy can be improved by pre-treatment in cerium solution. Živković et al. [47] revealed that the corrosion resistance of powder polyester coating on AA6060 can be improved by pre-treatment of substrate via Ce-based coating. S. Živković et al. [48] revealed the enhancement of the Protective properties of cataphoretic epoxy coating on aluminum alloy AA6060 modified with electrodeposited Ce-based coatings. Golabadi et al. [49] showed the effect of La containing PEO pretreatment on the protective performance of epoxy coating on magnesium.

Based on the results of several researches, using organic and inorganic inhibitors can lead to the formation of organic-inorganic complexes, which improves the corrosion resistance of the substrate. Organic additives initially act through adsorption on the metal surface and at the end may lead to the formation of metal/organic complexes [50,51]. The effectiveness of this phenomenon depends on the presence of polar functional groups with sulfur, oxygen or nitrogen heteroatoms in their molecular structure, heterocyclic compounds, and π electrons [52]. Herbal inhibitors as a subset of organic additives have attracted lots of attention because of their abundant, ecological acceptance, renewability, accessibility and non-toxic nature [53,54]. In this regard, the extract of Urtica leaf as a green inhibitor has been shown as an acceptable corrosion inhibitor of mild steel in acid solution [55–57]. This extract contains different inhibitive compounds i.e. Quercetin, Hystamine and Serotonin [58,59]. These compounds include several functional groups i.e. phenol, hydroxyl and carboxyl which are considered as main centers of adsorption on the metal surface. It is expected to form Ce film with more density and lower crack and defect on the steel surface. Also, the presence of many functional groups, i.e NH_2 and OH, in the organic compounds existed in the Urtica leaf extract can results in the establishment of strong chemical bonds between the polar groups of epoxy coating and steel substrate.

The aim of this study is to modify the cerium conversion coating by a post-treatment bath of Urtica extract and to investigate its effect on the adhesion and corrosion protection properties of the epoxy coating. To the best of authors' knowledge there is no study conducted on the effect of a secondary bath of green corrosion inhibitor on the cerium conversion coating properties. For this purpose, the steel substrates were firstly treated by a cerium conversion bath and then post-treated by a bath of Urtica extract. For finding the best conditions of the post-treatment bath, the chemical treatment was performed at various times and pHs. Corrosion resistance of the obtained coatings was investigated by means of electrochemical impedance spectroscopy (EIS) and the coating with superior resistance was chosen as the optimum sample. For surface characterizing, scanning electron microscopy (SEM), energy dispersive spectroscopy (EDS), contact angle (CA) and atomic force microscopy (AFM) measurements were performed on the coating synthesized in optimum conditions. Then the epoxy coating was applied on the aforementioned samples and its corrosion behavior was studied in the presence of an artificial defect through EIS and salt spray tests. Interfacial adhesion bonds between the epoxy and the conversion layer and its cathodic delamination behavior were also studied via pull-off and cathodic delamination tests, respectively.

2. Experimental

2.1. Materials

ST-12 plates (0.04 wt% Al, 0.05 wt% S, 0.05 wt% P, 0.32 wt% Mn, 0.34 wt% Si, 0.19 wt% C and 99.01 wt% Fe), with dimensions of 20 × 30 × 2 mm, were supplied by Foolad Mobarakeh Co (Iran). Cerium nitrate, $Ce(NO_3)\cdot 5H_2O$, and hydrogen peroxide, H_2O_2, were procured from Merck Co (Germany), and hydrochloric acid, HCl, and sodium hydroxide, NaOH, were prepared from Mojallali Co (Iran). Epoxy resin (bisphenol-A, with solid content of 74–76% and epoxy value of 0.1492–0.1666 Eq/100 g) with trade name of Araldite GZ 7071 × 75, and polyamide hardener with trade name of CRAYAMID 115 (solid content of 50% and density of 0.97 g/cm^3) were purchased from Saman and Arkema Co, respectively.

2.2. Urtica leaves extraction process

The fresh leaves of Urtica plant, which grows in the north of Iran, washed with tap water, dried in the shade and then powdered into small pieces. 20 g of the Urtica powder was added to 500 mL deionized water, placed on a magnetic stirrer for 3 h at a temperature of 70 °C and then passed through a filter paper. Again, the resulting solution was kept on the stirrer at a temperature of 40 °C until approximately most of the water evaporated. The remaining concentrated solution was dried by means of a heater. Based on literature [59] there are many organic/inorganic compounds like hystamine, serotonin, flavonal glycoside (quercitin and carotenoids), acids (e.g.carbonic and formic acid), chlorophyll, vitamins (C, B and K) and minerals (e.g. calcium, magnesium, and potassium)in the Urtica leaf extract. Among these Quercetin, Hystamine and Serotonin due to many OH and NH_2 groups are candidates for showing good corrosion inhibition properties.

2.3. Surface treatment process

The steel sheets were abraded by #400, #600, #800 and #1200 emery papers, then degreased and washed with acetone and distilled water, respectively. The cleaned samples were immersed in the cerium bath made up of 2 g/L $Ce(NO_3)_3{\cdot}5H_2O$, 0.6 mL/L H_2O_2 and 11.5 mL/L HCl 37 wt.%. The treatment was performed for 5 min at room temperature (25 ± 5 °C) and pH = 3 (The pH was adjusted by adding few drops of NaOH 5 wt.% solution). The samples obtained were washed and then dried by air blowing. In the next step, the cerium treated samples were immersed in a post-treatment bath containing 400 ppm Urtica extract, 0.6 mL/L H_2O_2 and 11.5 mL/L HCl for different times of 2, 4 and 6 min and pHs of 4, 4.5 and 5. Again, the plates were washed with distilled water and dried in the air. The samples treated at different pHs and times are named as S(4:2 min), S(4:4 min), S(4:6 min) and S(4.5:2 min).

2.4. Epoxy coating application

By mixing polyamide curing agent and epoxy resin with the ratio of 1:1.3 w/w, the epoxy coating was prepared. Then, using a film applicator, the coating was applied on the untreated, cerium treated (Ce) and the Ce post-treated by Urtica (Ce-Ur) samples. In the next step, the coated samples were kept at room temperature up to 24 h following by post-curing at 100 °C for 1 h. The wet and dry thicknesses of the films were 120 and 50 ± 5 µm, respectively.

2.5. Characterization

2.5.1. FT-IR analysis

The chemical composition of Urtica extract was investigated by a Fourier transform infrared (FT-IR) spectrometer model Perkin Elmer. The spectrum was recorded in the wavenumber range of 400–4000 cm^{-1} using KBr powder.

2.5.2. Surface characterization

The surface morphology and microstructure of different samples were examined by SEM/EDS (model Phenom ProX) analysis. The electron source of this device was CeB_6, and the images were recorded using backscatter electron detector at a voltage of 15 kV. The surface topology of the samples was analyzed by AFM analysis (in tapping mode) model Dualscope DS 95-200, DME, Denmark. Static contact angle measurement was performed using an OCA 15 plus type system. For this purpose, 1 µL distilled water, as probe liquid, was placed on the samples and the contact angles were determined after 20 s. The tests were carried out at temperature of 25 ± 2 °C and humidity of 30 ± 5%.

2.5.3. Pull-off adhesion measurements

Epoxy coatings were applied on the untreated, Ce and Ce-Ur treated samples. For measuring the values of adhesion strength, a Posi test-pull off adhesion tester (DEFELSKO) was used. The measurement was performed according to ASTM D4541 by gluing an aluminum dolly on the surface of the epoxy coating using a two-part Araldite 2015 (Huntsman advanced materials, Germany) adhesive. Then, the coating around the dolly was split and the dolly was pulled until detachment of the epoxy coating from the substrate with a normal speed of 10 mm/min. To ensure the measurements reproducibility, all tests were performed on three replications.

2.5.4. Cathodic disbondment test

Investigation of cathodic delamination rate of the applied epoxy coatings on the untreated, Ce and Ce-Ur treated samples was performed in 3.5 wt.% NaCl solution at pH = 10. For this aim, a hole with a diameter of 5 mm was made in the midpoint of the samples with 16 cm^2 area. Next, the samples as cathodes of an electrochemical cell were immersed in the test solution and polarized under a potential of −1.34 V (vs. Ag/AgCl reference electrode) for 24 h. After dismounting the cell from the samples, the average disbonded area was calculated. In order to assure the repeatability of the results, the measurements were carried out on three replications.

2.5.5. Salt spray test measurements

In order to evaluate the effect of Ce and Ce-Ur coatings on the corrosion behavior of the epoxy coating, salt spray test was used. Salt spray test was done according to ASTM B117 (NaCl 5 wt% solution), where the chamber temperature was 35 °C. To this end, the scratches with 2 mm width and 4 cm length were created on the samples coated with epoxy coating using a sharp surgery knife. In the next step, the samples with an angle of 45° were put in salt spray test chamber with continues spray of atomized 5.0 wt.% NaCl solution (pH 7.0, temperature 40 °C) continuously spraying on them.

2.5.6. EIS evaluation

The electrochemical impedance spectroscopy (EIS) measurement was performed by Autolab pgstat 302n electrochemical measurement equipment. For this purpose, the samples immersed in 300 mL of 3.5 wt.% NaCl solution at ambient temperature and a conventional three electrode cell was used for the measurement. The cell used consisted of the treated samples with an exposure area of 1 cm^2, a saturated calomel electrode (SCE) and a platinum mesh as working electrode, reference electrode and counter electrode, respectively. Furthermore, for investigating the corrosion behavior of the epoxy coating, the EIS analysis was adopted. For this aim an artificial scratch (20 mm in width) was created on the epoxy coated samples. Potentiodynamic measurements were started from cathodic to the anodic direction at ± 250 mV around OCP. The scan rate and perturbation for the polarization test was 1 mV/s and ± 10 mV, respectively. The frequency of the EIS measurement was in the range of 10 kHz to 10 mHz and the peak to zero amplitude was adjusted at ± 10 mV. It is worth to mention that as there was no linear Tafel region in the anodic branches the determination of anodic Tafel slopes (β_a) and I_{corr} was not possible according to the interpolation method. So the corrosion current density was defined as interpolation of the cathodic branch asymptote with the line which crosses the E_{corr}. The electrochemical data were recorded by the software package of Autolab workstation (Nova ver 1.7) and fitted using Zview software.

3. Results and discussion

3.1. Urtica extract characterization

The FT-IR spectrum of Urtica powder is shown in Fig. 1. In general, the vibration of O—H stretching is reported around 3500–3200 cm^{-1} which can be attributed to phenol or alcohol groups. In this work, the O—H stretching vibration is observed at 3417 cm^{-1} [60]. The presence of strong bands in the FT-IR spectra around 1800–1650 cm^{-1} is ascribed to the C=O stretching vibrations of saturated aliphatic or esters which can be seen here at 1650 cm^{-1} [60,61]. The absorption peak observed at 1130 cm^{-1} is attributed to the C—N stretching vibration of aliphatic amines [62], while 1430 cm^{-1} is probably due to the C—H bending vibration peak of $-CH_2$ [63]. Therefore, the Urtica extract is likely composed of aromatic rings and different functional groups of C=O, O—H, C—H and C—N. These results confirm the presence of different compounds i.e Hystamine, Serotonin and Quercetenin in the Urtica extract as reported in the literature [58,59].

3.2. Conversion coatings characterization

3.2.1. Surface characterization

3.2.1.1. SEM, EDS and AFM results. The surface morphology of the untreated, Ce and Ce-Ur treated samples are shown in Fig. 2. As can be

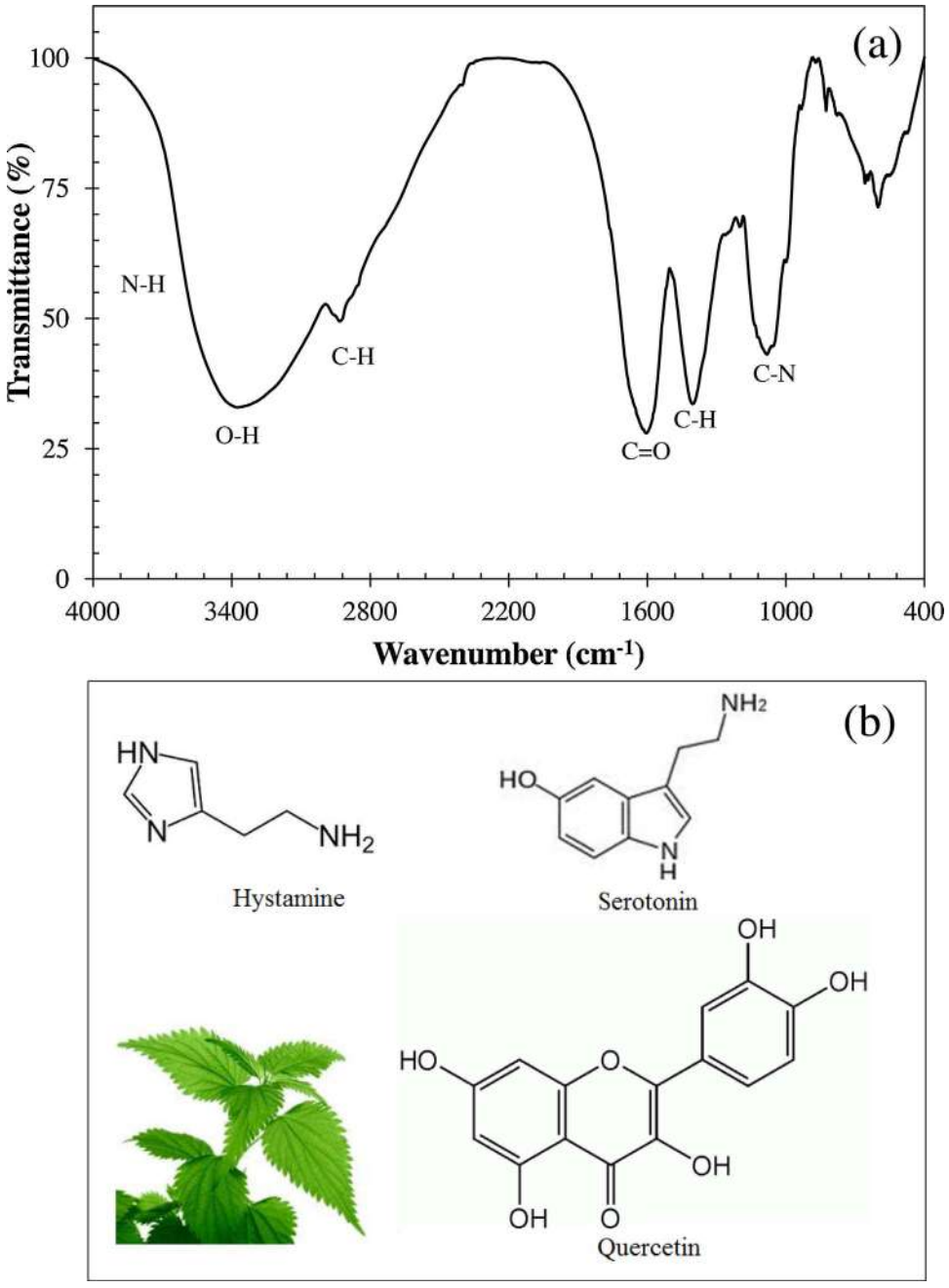

Fig 1. (a) FT-IR spectrum of Urtica extract; (b) chemical structure of three important inhibitive compounds present in the extract.

seen, by treating the steel substrate with Ce bath, a uniform layer of oxides and hydroxides, composed of CeO_2 and Ce_2O_3 [10], has covered the steel surface. However, he conversion layer contains high amount of micro cracks (as shown by the arrow in Fig. 2b_2) which is mainly due to the shrinkage of the film. The evolvement of trapped water molecules during the drying stage imposes extra-tension over the coating structure which leads to the coating cracking. By post-treating of the Ce sub-layer with inhibitor bath, however, the amount of micro cracks was diminished to a lower extent and a compact layer was formed on the surface. In fact, the inhibitor species filled the cracks and adsorbed/trapped in the porosities of the cerium sub-layer, resulting in the improvement of coating strength against stress release during drying step. Based on the EDS results, the amount of Fe was considerably reduced after treatment. In addition, the O content was increased along with detection of Ce in both Ce and Ce-Ur samples which is a sign of successful precipitation of the conversion layers consisted of cerium oxides/hydroxides. In the Ce-Ur sample, N was also detected due to the presence of organic compounds of the inhibitor. The roughness S_y (peak-peak height) and S_a (arithmetical mean height) were obtained from the AFM results for different samples. For the untreated sample the S_y and S_a are 52 and 3.2 nm, respectively. S_y and S_a of 67 and 8 nm were obtained for the Ce treated sample. For the sample treated by Ce-Ur the values of S_y and S_a were 102 and 8.5 nm, respectively. These results reveal that the formation of cerium layer and also the incorporation of inhibitor species significantly changed the topology of the steel surface and resulted in the increment of the surface roughness which is beneficial to enhance the adhesion properties of the epoxy coating applied on the steel surface.

3.2.1.2. Contact angle results. Contact angle measurement was performed in order to determine the effect of post-treatment on the surface chemistry of steel substrate. Nuemann's (Eq. (1)) and Young's (Eq. (1)) equations were employed to calculate the surface energy and work of adhesion:

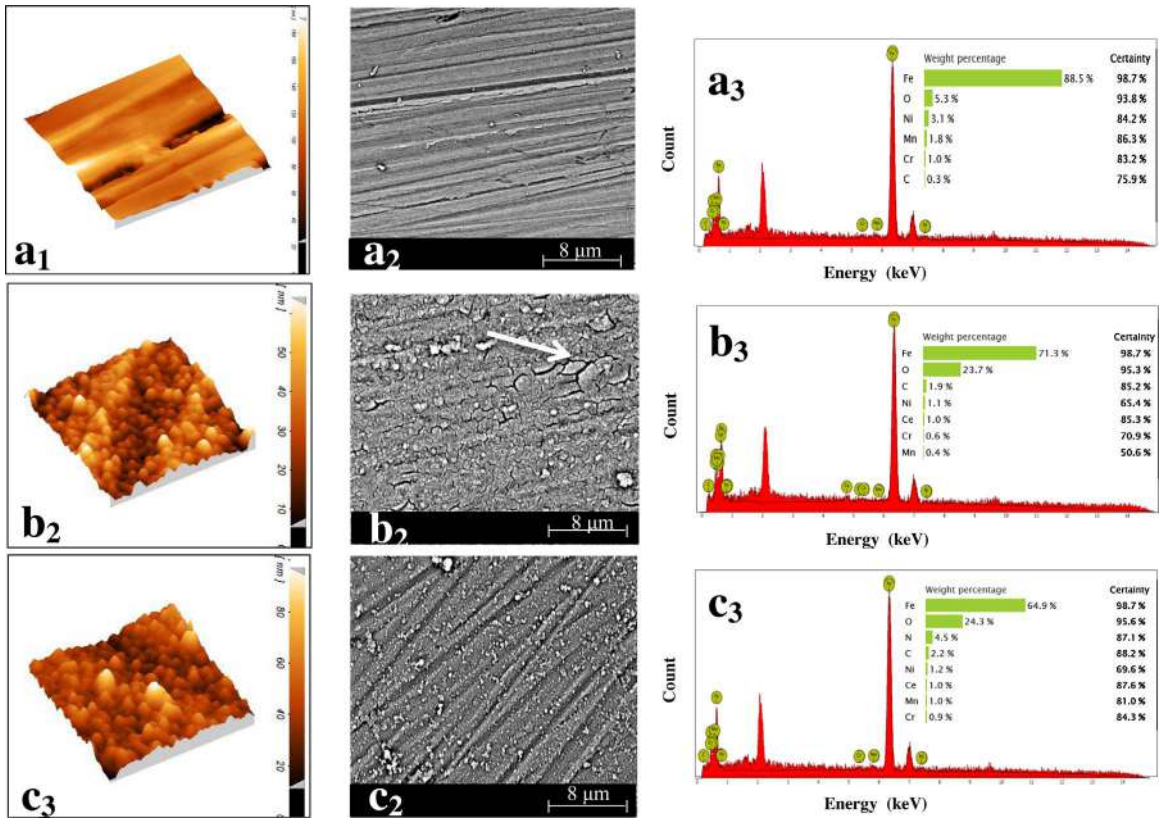

Fig. 2. (a_1, b_1, c_1) 3D AFM images, (a_2, b_2, c_2) SEM micrographs and (a_3, b_3, c_3) EDS spectra of the untreated sample, Ce treated sample at pH = 3 and t = 5 min and the Ce-Ur sample post-treated at pH = 4.5 and t = 6 min, respectively.

$$W_A = 2(\gamma_{lv}.\gamma_{sv})^{1/2}\exp[-\beta(\gamma_{lv} - \gamma_{sv})^2] \quad (1)$$

$$W_A = \gamma_{lv}(1 + \cos\theta) \quad (1)$$

where θ, γ_{lv} and γ_{sv} are the contact angle of water droplet, the surface tension of water, and the surface free energy of the substrate, respectively. β is considered as 0.0001247 ± 0.000010 $(mJ/m^2)^2$. The measurement was performed at three points of each sample and the results are the average of three values, as given in Fig. 3.

As can be seen from the result, by applying the Ce and Ce-Ur conversion coatings on the steel substrate the values of γ_s and W_a were increased, depicting the wettability and hydrophilicity enhancement. This can be due to the formation of more hydrophobic compounds on the steel surface such as $Ce(OH)_4$ and CeO_2 in the case of Ce sample and also metal/organic complexes in the case of Ce-Ur sample. In the case of the bare steel only the polar interactions i.e. hydrogen bonds and van der Waals forces are responsible for the adhesion bonds creation between the water molecules and metal surface. However, the interaction of steel surface treated by conversion film would be mostly in the form of primary chemical bonding, or chemisorption and these are strong interactions that are highly stable. Another reason can be the increase of surface roughness. The higher surface roughness results in the easier spread of water droplet on the surface.

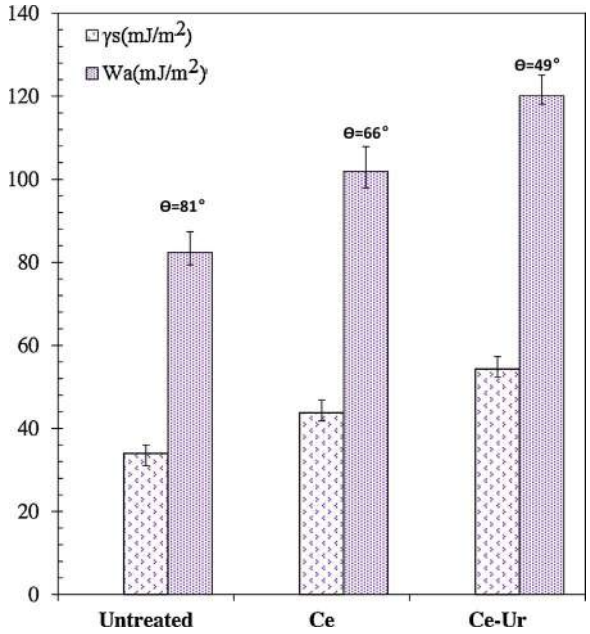

Fig. 3. Contact angle, surface free energy and work of adhesion values for various samples; the values are the mean of three replicates.

3.2.2. Corrosion studies

3.2.2.1. EIS measurements. The effect of environmental factors such as pH and immersion time on the adsorption of organic inhibitors is of great importance. Two factors were considered when selecting the pH of the post-treatment bath: i) the pH should be chosen in a way that the adsorption of the majority of the inhibitor compounds can take place; ii) the acidity of the post-treatment bath should not be too high to have undesirable effects on the cerium conversion coating morphology and to prevent the undesirable dissolution of deposited Ce oxide film. On the other hand, the time of post-treatment has a considerable effect on the amount of adsorbed Urtica species and also deterioration of the Ce film. In this respect, since the green corrosion inhibitor bath of Urtica is composed of different organic compounds with various functional groups that have a specific adsorption behavior, the effectiveness of the adsorption in different pHs of 4, 4.5 and 5 and post-treatment times of 2, 4 and 6 min have been investigated.

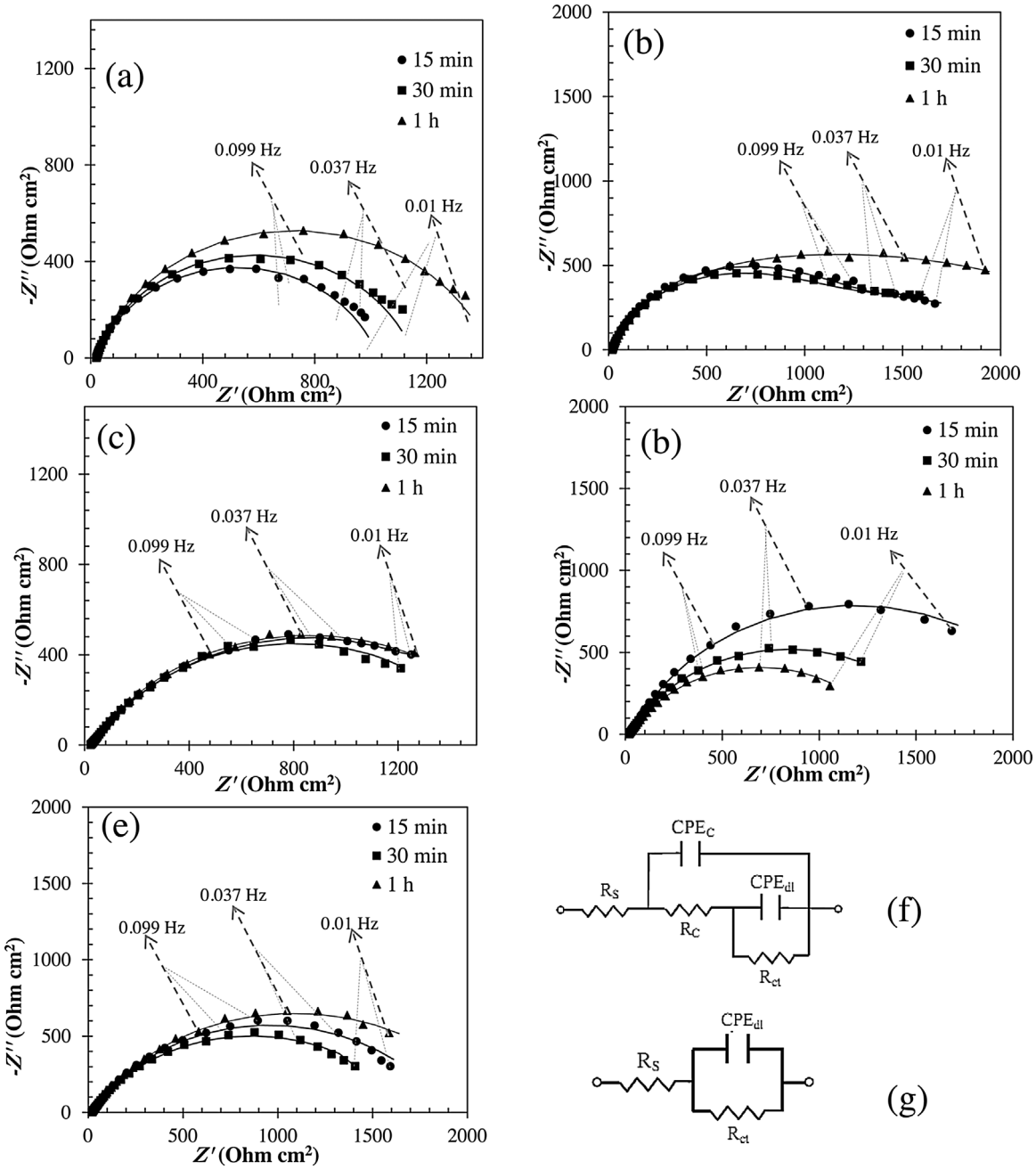

Fig. 4. Nyquist plots of (a) untreated, (b) Ce treated samples, (c) S(4:2 min), (d) S(4:4 min) and (e) S(4:6 min) samples (1 cm^2) exposed to 3.5 wt.% NaCl solution for 15, 30 and 60 min at room temperature. The marker points and solid lines show the experimental and fitted data, respectively. (f) and (g) show two and one time constants equivalent circuits.

EIS measurements were carried out after 15, 30 and 60 min immersion on the untreated, Ce and Ce-Ur treated samples in 3.5 w.t% NaCl solution. The Nyquist plots are shown in Figs. 4 and 5 and the data extracted are reported in Tables 1 and 2. One-time and two-time constant electrical equivalent circuits (EECs) were utilized for fitting the plots obtained. Due to the porosity of the conversion layers the constant phase element (CPE) was adopted instead of ideal capacitance (*C*) [64]. In the suggested EECs (Fig. 4f–g), the R_s, R_{ct}, R_c, CPE_c and CPE_{dl} are the solution resistance, charge transfer resistance, coating resistance and non-ideal capacitance of the coating and non-ideal capacitance of double layer, respectively. Y_0 and *n* are the admittance and exponent of CPE, respectively.

In the case of untreated steel, only one time constant can be observed, indicating that the electrode is under charge transfer control. Furthermore, a slight increase of the semicircle diameter has occurred with increasing the immersion time, which is attributed to the accumulation of corrosion products which could slightly restrict the transfer of electrical charge, leading to the R_{ct} rise. By applying CeCC on the bare steel, however, another time constant is appeared in high frequency which belongs to the cerium layer formed on the steel substrate. It can be seen that the total resistance ($R_t = R_{ct} + R_c$) of the modified steel is higher than that of untreated one, suggesting the successful precipitation of a barrier cerium oxide film. The increase in R_{ct} with exposure time in this case can be ascribed to the inhibition behavior of the Ce^{4+} species present in the coating structure, leading to the passivation of defected site and in this way it can prevent the corrosion of steel.

According to the extracted data, in the case of post-treated samples at various conditions, the highest R_{ct} and $|Z|_{10mHz}$ is related to pH = 4.5 and t = 6 min while the sample treated in pH = 4 and

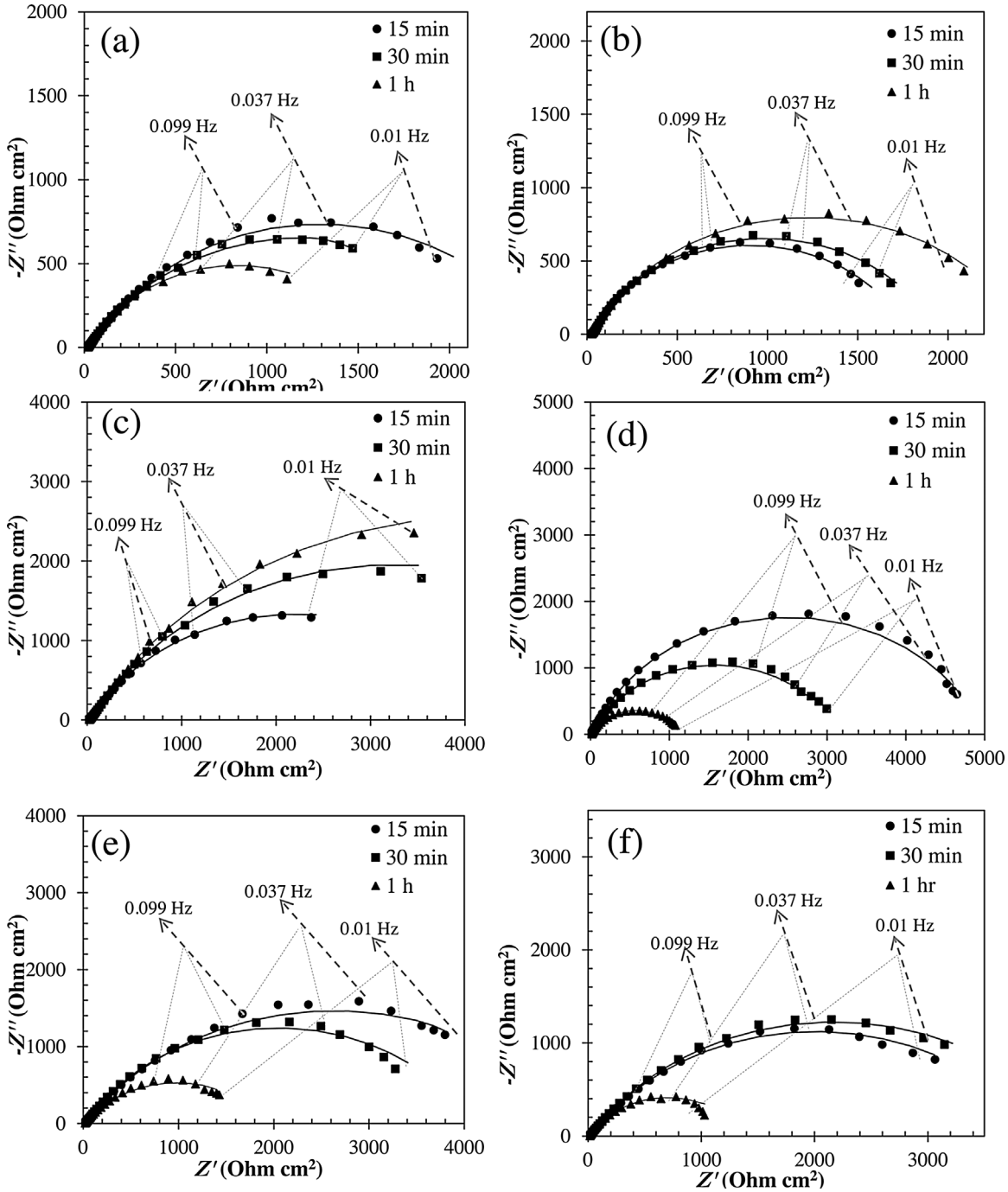

Fig. 5. Nyquist plots of (a) S(4.5:2 min), (b) S(4.5:4 min) and (c) S(4.5:6 min), (d) S(5:2 min), (e) S(5:4 min) and (f) S(5:6 min) samples (1 cm^2) exposed to 3.5 wt.% NaCl solution for 15, 30 and 60 min at room temperature. The marker points and solid lines show the experimental and fitted data, respectively.

Table 1
The electrochemical data obtained from impedance plots of untreated and Ce treated steel exposed to 3.5 wt.% NaCl solution for 15, 30 and 60 min at room temperature; the values are the mean of three replicates and (±) corresponds to the standard deviations.

Sample	Time (min)	R_{ct} (Ω cm^2)	CPE		R_c (Ω cm^2)	CPE	
			Y_0 ($\mu\Omega^{-1}$ cm^{-2} s^n)	n		Y_0 ($\mu\Omega^{-1}$ cm^{-2} s^n)	n
Untreated	15	1007 ± 45	918 ± 52	0.81 ± 0.01	–	–	–
Untreated	30	1137 ± 65	947 ± 13	0.82 ± 0.02	–	–	–
Untreated	60	1414 ± 52	983 ± 28	0.81 ± 0.01	–	–	–
Ce treated	15	1930 ± 23	235 ± 47	0.71 ± 0.01	32 ± 12	438 ± 33	0.35 ± 0.01
Ce treated	30	2240 ± 12	625 ± 54	0.71 ± 0.02	15 ± 22	345 ± 54	0.36 ± 00.2
Ce treated	60	2900 ± 54	465 ± 76	0.70 ± 0.01	23 ± 8	479 ± 71	0.35 ± 0.02

Table 2
The electrochemical data obtained from impedance plots of different post-treated samples exposed to 3.5 wt.% NaCl solution for 15, 30 and 60 min at room temperature; the values are the mean of three replicates and (±) corresponds to the standard deviations.

Sample	Time (min)	R_{ct} (Ω cm^2)	CPE		R_c (Ω cm^2)	CPE		$\|Z\|_{10\ mHz}$ (Ohm cm^2)
			Y_0(μΩ^{-1} cm^{-2} s^n)	n		Y_0 (μΩ^{-1} cm^{-2} s^n)	n	
S(4:2 min)	15	1661 ± 134	387 ± 47	0.67 ± 0.01	40 ± 12	794 ± 33	0.64 ± 0.01	3.11 ± 0.08
S(4:2 min)	30	1528 ± 54	656 ± 54	0.67 ± 0.02	28 ± 22	804 ± 54	0.66 ± 00.2	3.09 ± 0.05
S(4:2 min)	60	1652 ± 82	604 ± 76	0.70 ± 0.02	26 ± 8	1132 ± 71	0.65 ± 0.02	3.12 ± 0.07
S(4:4 min)	15	2298 ± 148	1105 ± 22	0.78 ± 0.01	22 ± 43	690 ± 94	0.72 ± 0.01	3.25 ± 0.10
S(4:4 min)	30	1600 ± 125	787 ± 74	0.73 ± 0.03	42 ± 4	1419 ± 19	0.71 ± 0.03	3.11 ± 0.08
S(4:4 min)	60	1272 ± 163	640 ± 37	0.71 ± 0.01	71 ± 54	1465 ± 47	0.69 ± 0.04	3.03 ± 0.07
S(4:6 min)	15	1885 ± 30	486 ± 29	0.63 ± 0.02	31 ± 21	344 ± 10	0.78 ± 0.02	3.21 ± 0.06
S(4:6 min)	30	1688 ± 93	710 ± 85	0.62 ± 0.01	17 ± 20	318 ± 39	0.80 ± 0.01	3.15 ± 0.11
S(4:6 min)	60	2108 ± 46	552 ± 90	0.64 ± 0.01	33 ± 8	855 ± 68	0.73 ± 0.04	3.22 ± 0.09
S(4.5:2 min)	15	2314 ± 39	211 ± 69	0.71 ± 0.01	228 ± 12	752 ± 15	0.65 ± 0.02	3.30 ± 0.05
S(4.5:2 min)	30	2197 ± 50	120 ± 55	0.86 ± 0.02	163 ± 19	1180 ± 27	0.63 ± 0.02	3.19 ± 0.04
S(4.5:2 min)	60	1582 ± 94	659 ± 49	0.80 ± 0.02	17 ± 4	1724 ± 84	0.66 ± 0.01	3.07 ± 0.09
S(4.5:4 min)	15	1719 ± 16	577 ± 40	0.81 ± 0.03	45 ± 10	611 ± 90	0.73 ± 0.01	3.18 ± 0.05
S(4.5:4 min)	30	1888 ± 167	611 ± 58	0.78 ± 0.01	23 ± 66	461 ± 20	0.74 ± 0.02	3.23 ± 0.08
S(4.5:4 min)	60	2379 ± 159	399 ± 77	0.77 ± 0.02	25 ± 34	471 ± 43	0.72 ± 0.02	3.32 ± 0.11
S(4.5:6 min)	15	3514 ± 48	214 ± 83	0.86 ± 0.01	1227 ± 11	435 ± 81	0.67 ± 0.01	3.43 ± 0.06
S(4.5:6 min)	30	6385 ± 136	471 ± 66	0.72 ± 0.02	61 ± 24	486 ± 23	0.67 ± 0.01	3.59 ± 0.04
S(4.5:6 min)	60	8314 ± 71	566 ± 40	0.72 ± 0.02	38 ± 19	532 ± 29	0.68 ± 0.02	3.62 ± 0.09
S(5:2 min)	15	4901 ± 247	284 ± 64	0.78 ± 0.02	74 ± 54	163 ± 51	0.78 ± 0.01	3.67 ± 0.10
S(5:2 min)	30	3139 ± 184	290 ± 12	0.67 ± 0.02	63 ± 71	192 ± 10	0.77 ± 0.03	3.48 ± 0.07
S(5:2 min)	60	1106 ± 46	545 ± 32	0.73 ± 0.01	–	–	–	3.03 ± 0.10
S(5:4 min)	15	5224 ± 93	448 ± 65	0.65 ± 0.02	24 ± 10	328 ± 17	0.59 ± 0.01	3.59 ± 0.06
S(5:4 min)	30	4003 ± 19	104 ± 22	0.76 ± 0.01	38 ± 24	440 ± 33	0.69 ± 0.01	3.52 ± 0.04
S(5:4 min)	60	1924 ± 55	1050 ± 87	0.63 ± 0.02	–	–	–	3.16 ± 0.09
S(5:6 min)	15	3999 ± 228	323 ± 76	0.62 ± 0.02	16 ± 6	302 ± 74	0.68 ± 0.02	3.50 ± 0.04
S(5:6 min)	30	4324 ± 84	382 ± 44	0.63 ± 0.03	43 ± 33	259 ± 52	0.69 ± 0.02	3.51 ± 0.02
S(5:6 min)	60	1361 ± 63	1391 ± 64	0.69 ± 0.02	–	–	–	3.02 ± 0.13

t = 6 min has the lowest values. For pH = 5 at all treatment times, the R_{ct} has an intense increase up to 30 min immersion and significant decrease after 1 h.

As it was expected, the corrosion behavior of the Ce-Ur treated samples considerably depends on the pH of the post-treating Urtica bath solution and this can be ascribed to the degree of inhibitors entailment within the CeCC. Results show that the corrosion resistance of the Ce-Ur treated sample obtained at pH = 4 and at almost all post-treatment times is approximately equal to and in some cases less than that of the Ce sample. As a result, it can be concluded that the slight dissolution of cerium oxide film may take place at this acidic pH and thus the increment of the exposed areas of the bare steel has occurred due to the excessive acidity of the inhibitor bath, leading to lower R_{ct} and $|Z|_{10mHz}$ values. On the other hand, the inhibitor species do not show an effective entailment and/or adsorption in the Ce film in this particular pH because of the intensive protonation of inhibitor molecules which reduces their tendency to adsorb into the coating. At pH = 4.5, the R_{ct} and $|Z|_{10mHz}$ values are approximately equal in almost all immersion times and in some cases are higher compared with Ce sample. It can be seen that the total resistance (R_t) increases by increasing the treatment time so that a significant increase is observed in S (4.5, 6 min). The fact that highly attracts the attention here is the increase of R_t with increasing the immersion time. It can suggest that by immersing the Ce-Ur treated sample in 3.5 wt.% NaCl solution during EIS measurement, the trapped inhibitors in the porosities of CeCC gradually release and dissolve in NaCl solution and therefore provide inhibitive action for the coating system. Oxygen and nitrogen heteroatoms present in the inhibitor structure, i.e Hystamine and Serotonin, are electron rich elements. The lone-pair orbitals of nitrogen and oxygen heteroatoms and/or molecular π-system are capable of creating organic-inorganic hybrids with Fe cations through interaction with its partially occupied d-bands (Eq. (3)).

$$Fe^{2+} + mH_2O + nCl^- + pInh \rightarrow [Fe(Inh)_p(OH)_m(Cl)_n]^{2-m-n} + m(H)^+ \quad (3)$$

In optimum conditions, the complex precipitates on the steel surface, otherwise it will dissolve. It is also reported that adsorption of heterocyclic compounds along with aromatic cycles can occur sometimes parallel but frequently normal to the steel surface. These complexes occupy a large surface area, thus cover the exposed sub-layer and protect it from corrosive agents' attacks [65]. As a result, not only the corrosion can be inhibited on the anodic areas but also due to the formation of complexes the resistance increases by immersion time. This fact is confirmed by EIS results where the increase in R_t is mostly due to the R_{ct} increment rather than R_c.

At pH = 5 the increase in R_t and $|Z|_{10mHz}$ is most significant compared to other pHs at the beginning of immersion. However, after 60 min immersion the resistance drops considerably. Accordingly, the Ce-Ur samples treated for 2 and 4 min have R_t and $|Z|_{10mHz}$ less than the Ce treated sample after 60 min immersion. The Bod plots for this condition consist only one time constant which can be attributed to the deterioration of the conversion layer. In this case the adsorption of the inhibitors was mostly taken place in the cracked areas of the CeCC but soon after exposure to NaCl solution the inhibitors leave the coating. Therefore the coating significantly loses its protection performance after 60 min immersion. Therefore, corrosion occurs intensely in the bare exposed areas of the steel substrate.

Based on the above analysis, the influence of pH of post treatment bath on the CeCC properties in a same post-treatment time, for example t = 6 min, can be schematically illustrated by Fig. 6. The scheme shows that, at pH = 4 no inhibitor traps in the Ce sub-layer, therefore the bare steel especially within the cracks is exposed to the corrosive electrolyte thus the coating deteriorates with time. At pH = 4.5, however, the inhibitors trapped within the coating produce complexes with iron substrate hence protecting the layer against corrosion attacks during the exposure. At pH = 5, the inhibitors adsorbed in the cracks gradually desorb when the coating is immersed in the corrosive solution thus the corrosion occurs again. According to the above statements, the Ce-Ur sample treated for 6 min in pH = 4.5 has an improved performance and significant inhibition behavior compared with other samples.

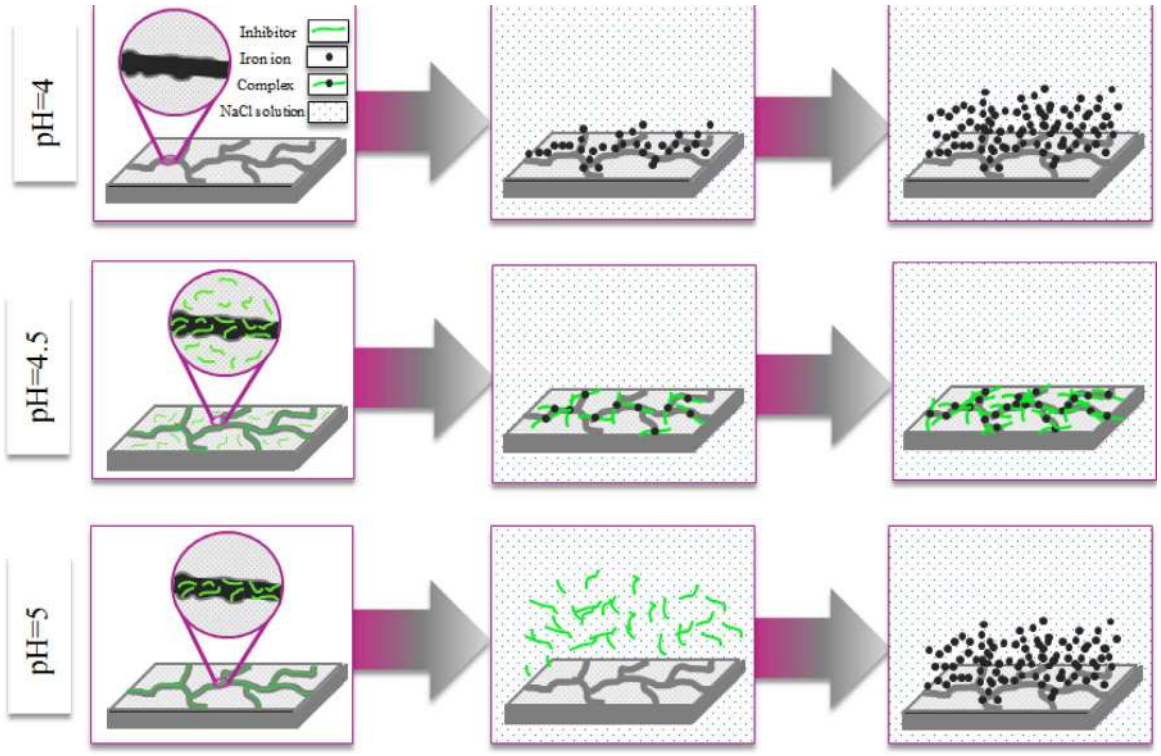

Fig. 6. Schematic representations of the influence of pH of the Urtica post-treatment bath on the Ce-Ur properties.

Therefore, this sample was chosen as a substrate for further characterization of corrosion resistance and adhesion properties of the epoxy coating.

3.3. Epoxy coating characterization

3.3.1. EIS measurement

In order to evaluate the effect of surface treatment of steel on the corrosion protection properties of the epoxy coating, the EIS measurement was carried out on the epoxy coating applied on the treated/untreated samples. The test was performed on the sample with an artificial defect at OCP in 3.5 wt.% NaCl solution for different immersion times of 3, 6, 12 and 72 h. The defects with the same length (20 mm) and width were produced on all coatings by a sharp surgery knife. The Nyquist and Bod plots are shown in Fig. 7 and the results obtained are reported in Table 3.

When an epoxy coating experiences a defect, the coating delamination initiates from this region. As can be seen from the impedance data, the untreated sample has the lowest R_{ct} and $|Z|_{10mHz}$ at all immersion times and there is a slight increase in R_{ct} after 12 h immersion. By applying the CeCC on the steel surface, the R_{ct} and $|Z|_{10mHz}$ increased compared with the untreated substrate and slowly decreased with immersion time. However, in the case of Ce-Ur sample the improvement of R_{ct} was more significant and a little reduction is observed with immersion time. In fact, the decrease of R_{ct} is an indicator of the epoxy coating disbonding from the substrate as a result of the electrolyte diffusion to the coating/metal interface, resulting in the higher coating delamination and hence lower R_{ct} values. In the case of the untreated sample the coating delamination and corrosion products development beneath the coating occur intensely due to the poor adhesion of the epoxy coating to the untreated substrate. However, the accumulation of corrosion products after 12 h in the defect site resulted in slight increase of R_{ct}. In the case of CeCC sample the stronger bonding of epoxy/substrate led to the higher initial value of R_{ct} and $|Z|_{10mHz}$ but the adhesion bonds deterioration took place at longer immersion times, leading to the decrease of R_{ct} and $|Z|_{10mHz}$. However, the adhesion bonds in the Ce-Ur sample are more stable and due to the inhibition role of Urtica molecules adsorbed in the Ce film the highest values of R_{ct} and $|Z|_{10mHz}$ were obtained for this sample. It can be seen that the R_{ct} significantly decreased after 72 h exposure for all samples, but the Ce-Ur sample shows higher corrosion protection performance compared to the other samples.

3.3.2. Salt spray test results

The effect of surface treatment of steel samples by Ce and Ce-Ur conversion films on the corrosion protection properties of epoxy coating was evaluated by salt spray test and the results are given in Fig. 8. The test was performed on the samples with and without scratch after 500 and 1500 h exposure times, respectively. By scratching the coating (Fig. 8a), the steel becomes in direct exposure to the corrosive electrolyte and corrosion reactions initiate at the defect region. Two parallel anodic (dissolution of iron, $Fe \rightarrow Fe^{2+} + 2e$) and cathodic (oxygen reduction, $2H_2O + O_2 + 4e \rightarrow 4OH^-$) reactions occur in the scratch part. The OH^- ions produce as a result of cathodic reaction, leading to the increase of pH beneath the coating and providing an alkaline environment. This high pH locally attacks the organic coating at the polymer/metal interface, causing the hydrolysis and deterioration of the bonds between the polymer and metal, leading to the coating delamination and blistering. Then, the corrosion products creation results in further progress of disbonded area. Results show that surface modification of steel substrate affects the corrosion performance of the epoxy coating in a large extent. A little blister and corrosion product has appeared around the scratch of the Ce treated sample. Due to the dielectric nature of Ce film it can insulate the anodic and cathodic sites on the steel surface and in this way the rate of cathodic reaction can be noticeably reduced. As a result the lower pH rise takes place in the scratch part and beneath the coating. Therefore, the amount of blisters on the coating decreases. However, it is obvious that the Ce-Ur treated sample exhibits more acceptable results after 500 h salt spray. In comparison with the untreated and Ce treated samples, there are fewer blisters beneath the epoxy coating that was applied on the Ce-Ur treated substrate. Beside the mentioned beneficial effect of the Ce film, this

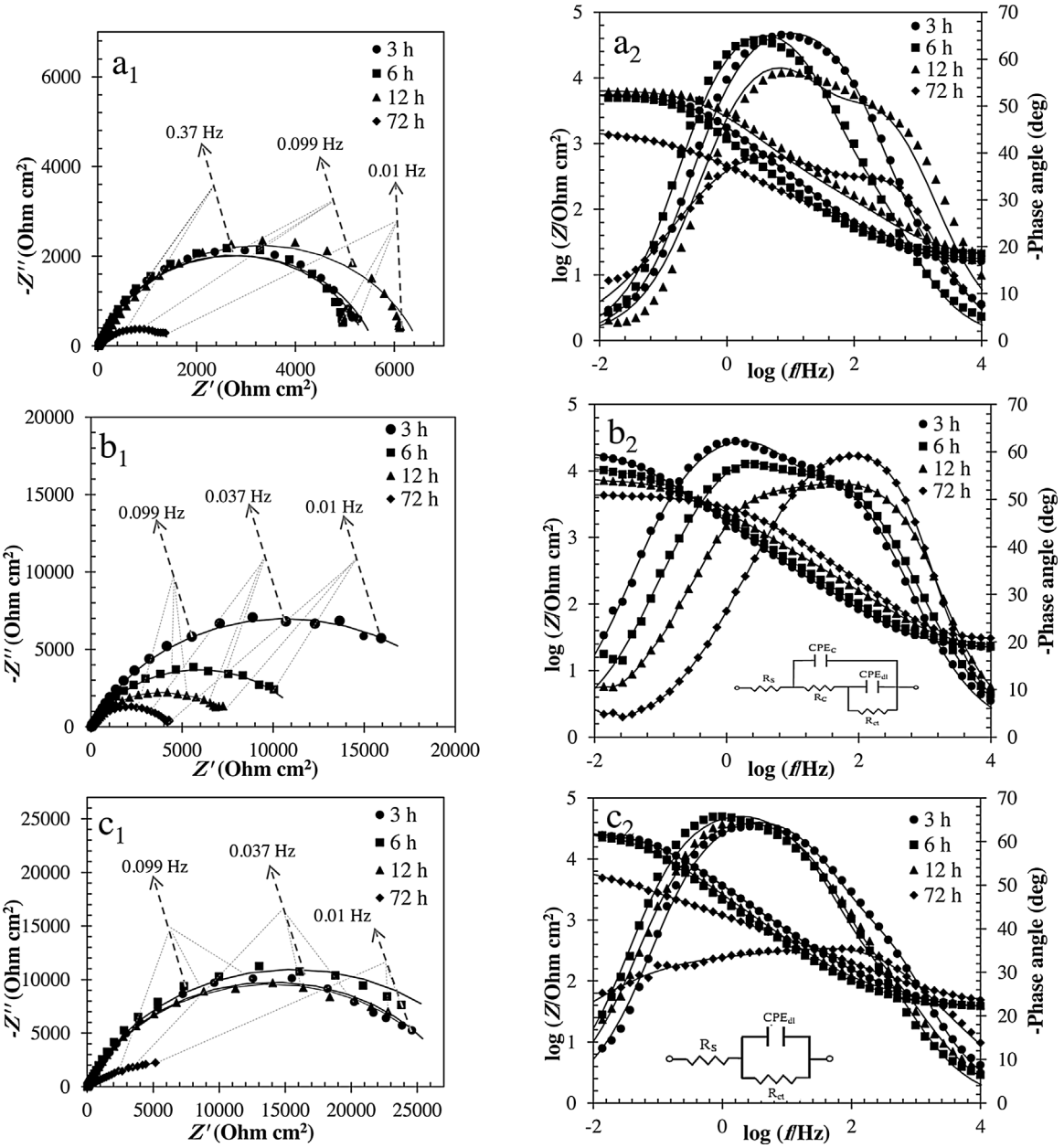

Fig. 7. Nyquist and Bode plots of epoxy with a scribe applied on (a_1 and a_2) the untreated, (b_1 and b_2) Ce and (c_1 and c_2) Ce-Ur samples exposed to 3.5 wt.% NaCl solution for 3,6, 12 and 72 h at room temperature. The data were normalized with respect to the total surface area (6 cm^2). The marker points and solid lines show the experimental and fitted data, respectively.

Table 3
The electrochemical data obtained from impedance plots of epoxy coated samples (with an artificial scribe) exposed to 3.5 wt.% NaCl solution for 3, 6, 12 and 72 h at room temperature.

Sample	Time (h)	R_{ct} (Ω cm^2)	CPE		R_c (Ω cm^2)	CPE		$\|Z\|_{10\ mHz}$ (Ohm cm^2)
			Y_0 ($\mu\Omega^{-1}$ cm^{-2} s^n)	n		Y_0 ($\mu\Omega^{-1}$ cm^{-2} s^n)	n	
Untreated	3	5571 ± 110	49 ± 34	0.78 ± 0.02	22 ± 8	64 ± 12	0.80 ± 0.02	3.71 ± 0.05
Untreated	6	5686 ± 124	77 ± 65	0.81 ± 0.02	67 ± 12	94 ± 15	0.81 ± 0.02	3.69 ± 0.07
Untreated	12	6103 ± 219	34 ± 24	0.78 ± 0.03	387 ± 19	46 ± 22	0.76 ± 0.03	3.78 ± 0.03
Untreated	72	1550 ± 234	651 ± 86	0.55 ± 0.02	51 ± 20	47 ± 16	0.83 ± 0.01	3.14 ± 0.11
Ce	3	21043 ± 352	34 ± 10	0.91 ± 0.02	340 ± 180	127 ± 65	0.72 ± 0.03	4.22 ± 0.09
Ce	6	11403 ± 405	102 ± 12	0.90 ± 0.01	518 ± 201	106 ± 30	0.74 ± 0.01	4.02 ± 0.08
Ce	12	7594 ± 343	156 ± 7	0.90 ± 0.02	379 ± 89	141 ± 22	0.76 ± 0.01	3.86 ± 0.04
Ce	72	3946 ± 109	90 ± 29	0.91 ± 0.01	513 ± 69	183 ± 43	0.74 ± 0.01	3.63 ± 0.08
Ce-Ur	3	27747 ± 603	105 ± 23	0.78 ± 0.01	242 ± 20	23 ± 4	0.76 ± 0.01	4.40 ± 0.12
Ce-Ur	6	30855 ± 21	154 ± 34	0.78 ± 0.01	127 ± 31	64 ± 11	0.78 ± 0.01	4.39 ± 0.07
Ce-Ur	12	27703 ± 284	219 ± 72	0.78 ± 0.01	120 ± 18	83 ± 18	0.75 ± 0.02	4.37 ± 0.10
Ce-Ur	72	13098 ± 401	343 ± 54	0.39 ± 0.03	631 ± 45	57 ± 20	0.55 ± 0.04	3.75 ± 0.05

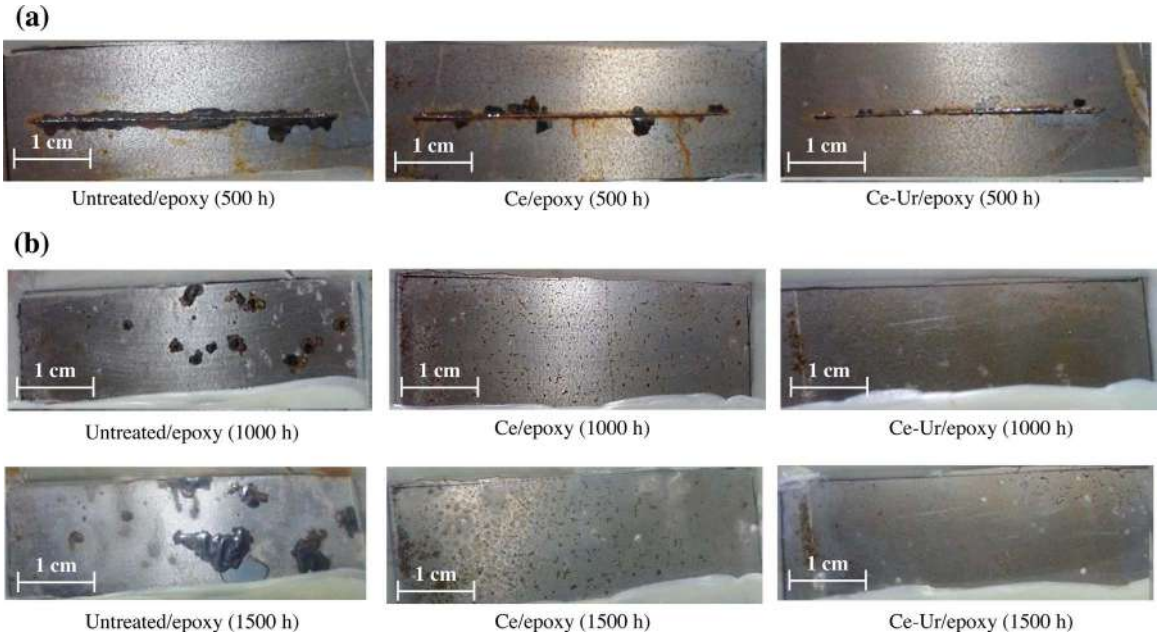

Fig. 8. Visual performance of (a) the epoxy coatings with a scribe after 500 h salt spray test and (b) the epoxy coatings without defect after 1000 and 1500 h salt spray test.

observation confirms the effective role of inhibitor incorporation on the corrosion protection performance of the epoxy coating. As it has been shown, the presence of Urtica molecules in the Ce-Ur film provides an inhibition property, which retards the corrosion reactions at anodic sites within the scratch and in this way a protective film can be deposited on the steel surface. The film deposited can block the active anodic and cathodic sites from the access of corrosive agents, leading to the decrease of hydroxyl ion generation in cathodic areas and therefore the amount of blistering and disbondment significantly decreases.

Fig. 8b shows the result of salt spray test for the coatings without defect after 1000 and 1500 h exposure. It shows large spots of corrosion products accumulations at the epoxy/steel interface for the untreated sample. The epoxy coating inherently contains microscopic pores and defects which are conductive pathways for diffusion of water, oxygen and ions into the coating matrix. As it is evident from Fig. 8b, the electrolyte diffusion does not take place uniformly but along the boundaries of the structural units of the epoxy coating. Such diffusion to the untreated steel has severely damaged the molecular network structure of the epoxy coating and dropped the efficiency of the coating protective performance. However, the amount of blistering and corrosion products in the case of Ce sample is far less than that of untreated sample and is in a scattered form. It can suggest that the conversion coating has created a barrier layer against water and ions diffusion in most areas. However, in the cracked regions (as it was shown in the SEM image) more and easier diffusion can occur which leads to the scattered blistering. Results show no significant corrosion products creation beneath the epoxy coating applied on the sample treated by Ce-Ur conversion coating. In the case of Ce-Ur treated sample, in addition to the reduced cathodic activity of the surface and active inhibition behavior, the improved performance can be attributed to the compactness and lesser amount of the micro-cracks of the conversion layer. As a result, the channels of diffusion or in the other words, the access of corrosive agents to the sub-layer have been considerably reduced.

3.3.3. Pull-off adhesion and cathodic disbondment test results

The effect of Ce and Ce-Ur treatments on the epoxy/steel interfacial bonding was evaluated by means of pull-off test in dry state and cathodic disbondment measurements. The results obtained are reported in Fig. 9.

As can be seen from the pull-off test results (Fig. 9a), two forms of failure occurred on different samples, namely adhesive failure and cohesive failure. In the case of cohesive failure, the disbondment takes place in the internal layers of the epoxy coating while in the adhesive one, the disbonding initiates along the epoxy/substrate interface. As a result, observation of cohesive failure instead of adhesive failure is the sign of adhesion improvement between the epoxy and substrate. It is evident from the images that by applying CeCC on the steel substrate the area of adhesive failure reduced compared with the untreated sample. On the other hand, a combination of cohesive and adhesive failures was observed in the Ce-Ur sample with less area of adhesive failure. Furthermore, the adhesive strength of the epoxy coating applied on this sample is more than others. This improvement can be ascribed to the higher roughness and surface free energy (i.e. wettability) of the surface modified with Ce-Ur. The epoxy coating has polar nature due to the presence of ether and hydroxyl groups in its chemical structure. The more hydrophobicity of the Ce-Ur sample helps the establishment of stronger adhesive polar-polar bonds between the epoxy coating and modified substrate. The higher surface roughness also leads to the more mechanical inter-locking between the epoxy and sub-layer by providing the organic coating with more anchors.

The effect of chemical modification of the steel surface by Ce and Ce-Ur on the cathodic disbondment rate of the epoxy coating is shown in Fig. 9b. As can be seen, the maximum amount of disbonding diameter belongs to the steel surface without any treatment. The results show that the chemical treatment by Ce and Ce-Ur noticeably reduced the disbondment rate compared to the untreated steel sample. This observation can be ascribed to the stronger adhesive bonds between the epoxy coating and the chemical treated substrates. In addition, the cerium oxide compounds have a high resistance in alkaline environments and also they reduce the cathodic activity of the metal surface by limiting the electron transfer from the anodic to cathodic sites and thus the rate of hydroxyl ions formation can be noticeably diminished. Application of secondary inhibitor bath further reduced the cathodic disbonding rate, which means further reduction of the cathodic activity of the steel surface. The remarkable inhibition property of the Ce-Ur coating, which was confirmed earlier, can play a major role in holding down the rate of production of hydroxyl ions beneath the epoxy coating. These results confirm that the inhibitor could effectively reduce the disbondment of epoxy coating on the steel surface.

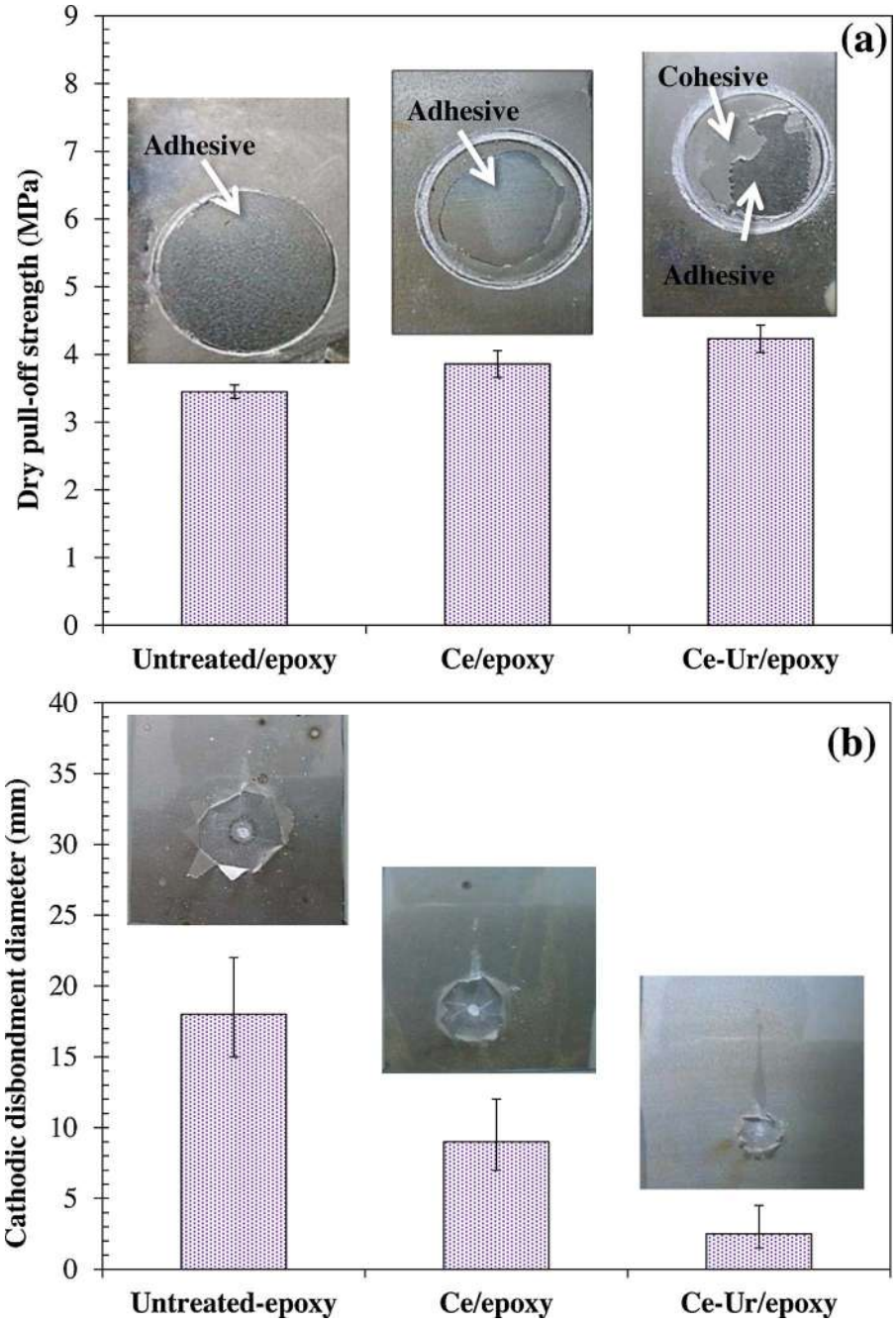

Fig. 9. Visual performance of the epoxy coatings applied on various samples after (a) pull-off measurement in dry state and (b) cathodic disbondment test; the values are the mean of three replicates and (±) corresponds to the standard deviations.

3.4. The mechanism of the effect of Urtica inhibitor on the type of bonding

In the case of untreated steel the bonding mechanism is based on weak physical bonds and electromagnetic bonding (hydrogen bonds). The polar groups existed in the epoxy coating, i.e epoxide and hydroxyl, can interact with hydrated metal oxides exist on the metal surface. These interactions are not strong and stable in corrosive environments. The water molecules diffuse into the coating/metal interface and significantly destroy the hydrogen bonds. The water molecules are strong hydrogen bonding agent, forming weak water layer at the polymer/metal interface and results in the adhesion bonds destruction [66–68]. The increase of pH at the coating/metal interface takes place as a result of hydroxyl ions creation on the cathodic sites and diffusion of Na^+ cations, forming NaOH which is a strong alkaline agent. The increase of pH results in further hydrogen bonds destruction and coating delamination. In the case of steel surface treatment by Ce solution combination of three (Ce_2O_3) and tetravalent (CeO_2) cerium oxides covers the steel surface (Eqs. (4)–(7)). The composition of these oxides has been studied by X-ray photoelectron spectroscopy (XPS) in our previous study [69].

$$4Ce^{3+} + O_2 + 6H_2O \rightarrow 4Ce(OH)_2{}^{2+} + 4H^+ \quad (4)$$

$$Ce^{3+} + 3OH^- \rightarrow Ce(OH)_3 \quad (5)$$

$$Ce(OH)_2{}^{2+} + 2OH^+ \rightarrow CeO_2 + 2H_2O \quad (6)$$

$$Ce(OH)_3 \rightarrow CeO_2 + H_2O + H_2 \quad (7)$$

Strong adhesion bonds with high durability in wet conditions can be created between the epoxy chains and steel surface through chemical treatment of metal surface by stable cerium oxides (CeO_2) film. The CeO_2 film increases the nanometric surface roughness, providing greater surface area and higher number of adhesion sites for the epoxy

coating. The epoxy chains can diffuse into the pores and cavities of Ce film, providing stronger physical interactions through mechanical interlocking. The increase of surface free energy and work of adhesion is another effect of Ce film deposition on the steel surface, enhancing the wettability of steel surface by epoxy polymer. Also, the strong chemical bonds can be obtained through interaction of Ce oxide and polar groups of epoxy coating like epoxide groups. The Ce film mostly covers the cathodic sites of metal surface and decreases the cathodic reaction rate. The Ce oxides insulate the steel surface and in this way reduce the electron transfer from anodic regions to cathodic sites. So, the rate of cathodic reaction can be decreased and lower pH rise can be seen at the steel/polymer interface. Therefore, the adhesion bonds destruction and coating delamination rates can be remarkably reduced. However, the electrolyte can diffuse into the cracks of Ce film, reaching the Ce film/steel interface and results in the coating deterioration. Addition of Urtica inhibitor to the Ce solution resulted in the precipitation of Ce film with lower cracks. In fact, as it has been previously stated the organic compounds existed in the Urtica extract, i.e Quercetin, Hystamine and Serotonin, can interact with Ce^{3+} cations, forming organic/inorganic complexes. This results in the Ce film shrinkage reduction during the coating drying stage and therefore lower cracks can be created. This is not the only mechanism. The organic compounds like Quercetin, Hystamine and Serotonin include many NH_2, C═O and OH groups in their structure. The lone pair electron of heteroatoms like N and O can be shared with empty orbital of Ce^{3+} and Ce^{4+} cations, forming different organic/inorganic complexes [70].

$$2\text{Urtica-OH} + Ce^{3+} \rightarrow \text{Urtica-HO-}\ Ce^{3+}\text{-OH-Urtica} \quad (8)$$

$$2\text{Urtica-NH}_2 + Ce^{3+} \rightarrow \text{Urtica-H}_2\text{N-}\ Ce^{3+}\text{-NH}_2\text{-Urtica} \quad (9)$$

Through a cation exchange mechanism the Ce^{3+} cations in the complexes can be replaced with Fe^{2+} cations, forming Urtica-HO-Fe^{2+}-OH-Urtica and Urtica-H_2N- Fe^{2+}-NH_2-Urtica complexes. The released Ce^{3+} cations can show inhibitory role when the corrosive electrolyte diffuses into the epoxy/metal interface, restricting the cathodic reaction and decreasing the pH. Therefore, lower interfacial adhesion bonds destruction occurs. Another role of Urtica-H_2N- Ce^{3+}-NH_2-Urtica and Urtica-HO-Ce^{3+}-OH-Urtica complexes is establishment of strong adhesion bonds between the steel surface and epoxy coating. First, the polar groups of Urtica can interact with polar groups of epoxy, providing strong electromagnetic bonding (hydrogen bonds). Second, the NH_2 groups of the hystamine and serotonin can interact with epoxide group of epoxy resin, forming strong chemical bonds through ring opening reaction. All of these results in the establishment of strong and stable physical and chemical bonds between the Ce-Urtica and epoxy matrix.

4. Conclusion

The CeCC sub-layer applied on the steel surface was modified by a post-treatment bath of green corrosion inhibitor at different pHs of 4, 4.5 and 5 and various post-treatment times of 2, 4 and 6 min. Different analytical techniques were adopted for characterization of the optimum condition to achieve promising corrosion and adhesion properties of the epoxy coating applied on it. The results obtained are as follow:

(1) The herbal extract was investigated by FT-IR analysis and it was found that it contains aromatic rings and functional groups such as C═O, O—H, C—H and C—N which are effective compounds to act as corrosion inhibitor.
(2) Based on the polarization and EIS results, the CeCC post-treated at pH = 4.5 and t = 6 min showed superior corrosion resistance and active inhibition property which was evident by decrease in i_{corr} and increase in R_{ct} with immersion time, respectively compared with the CeCC and untreated steel.
(3) Results showed that post-treatment of the CeCC with inhibitor bath at pH = 4.5 and t = 6 min led to the film with highest compactness and lowest micro-cracks. The increase of the surface roughness, the decrease of the contact angle and therefore the increase of the surface free energy and work of adhesion were seen after post-treatment of Ce with inhibitor bath. These all resulted in the improvement of the adhesion between epoxy and steel substrate.
(4) Incorporation of inhibitor species helped the reduction of the cathodic activity of surface and hydroxyl ion generation in the presence of corrosive electrolyte. Therefore a little amount of blistering was created near the scribe of the epoxy coating applied on the post-treated sample compared with CeCC and untreated steel. In addition, the delamination rate of the epoxy coating was significantly reduced and the EIS results confirmed the higher resistance of the epoxy coating.

References

[1] X. Liu, J. Xiong, Y. Lv, Y. Zuo, Study on corrosion electrochemical behavior of several different coating systems by EIS, Prog. Org. Coat. 64 (2009) 497–503.
[2] B. Liu, Z.-g. Fang, H.-b. Wang, T. Wang, Effect of cross linking degree and adhesion force on the anti-corrosion performance of epoxy coatings under simulated deep sea environment, Prog. Org. Coat. 76 (2013) 1814–1818.
[3] B. Díaz, L. Freire, M. Mojío, X.R. Nóvoa, Optimization of conversion coatings based on zinc phosphate on high strength steels, with enhanced barrier properties, J. Electroanal. Chem. 737 (2015) 174–183.
[4] N. Rezaee, M.M. Attar, B. Ramezanzadeh, Studying corrosion performance, microstructure and adhesion properties of a room temperature zinc phosphate conversion coating containing Mn2+ on mild steel, Surf. Coat. Technol. 236 (2013) 361–367.
[5] Z. Zou, N. Li, D. Li, H. Liu, S. Mu, A vanadium-based conversion coating as chromate replacement for electrogalvanized steel substrates, J. Alloys Compd. 509 (2011) 503–507.
[6] B. Ramezanzadeh, A. Ahmadi, M. Mahdavian, Enhancement of the corrosion protection performance and cathodic delamination resistance of epoxy coating through treatment of steel substrate by a novel nanometric sol-gel based silane composite film filled with functionalized graphene oxide nanosheets, Corros. Sci. 109 (2016) 182–205.
[7] J. Min, J.H. Park, H.-K. Sohn, J.M. Park, Synergistic effect of potassium metal siliconate on silicate conversion coating for corrosion protection of galvanized steel, J. Ind. Eng. Chem. 18 (2012) 655–660.
[8] B. Ramezanzadeh, M. Rostami, The effect of cerium-based conversion treatment on the cathodic delamination and corrosion protection performance of carbon steel-fusion-bonded epoxy coating systems, Appl. Surf. Sci. 392 (2017) 1004–1016.
[9] A. Eshaghi, A. Eshaghi, Effect of chromate conversion coatings on the adhesion and corrosion resistance of painted 5083 aluminum alloy, Mater. Sci. 48 (2012) 171–175.
[10] H. Vakili, B. Ramezanzadeh, R. Amini, The corrosion performance and adhesion properties of the epoxy coating applied on the steel substrates treated by cerium-based conversion coatings, Corros. Sci. 94 (2015) 466–475.
[11] G. Yoganandan, K. Pradeep Premkumar, J.N. Balaraju, Evaluation of corrosion resistance and self-healing behavior of zirconium–cerium conversion coating developed on AA2024 alloy, Surf. Coat. Technol. 270 (2015) 249–258.
[12] B. Ramezanzadeh, M.M. Attar, Cathodic delamination and anticorrosion performance of an epoxy coating containing nano/Micro-Sized ZnO particles on cr(III)-Co(II)/Cr(III)-Ni(II) posttreated steel samples, Corrosion 69 (2013) 793–803.
[13] B. Ramezanzadeh, M.M. Attar, Effects of Co(II) and Ni(II) on the surface morphology and anticorrosion performance of the steel samples pretreated by Cr(III) conversion coating, Corrosion 68 (2012) (015008-015001-015008-015011).
[14] B. Ramezanzadeh, M.M. Attar, M. Farzam, Corrosion performance of a hot-dip galvanized steel treated by different kinds of conversion coatings, Surf. Coat. Technol. 205 (2010) 874–884.
[15] R. Amini, H. Vakili, B. Ramezanzadeh, Studying the effects of poly (vinyl) alcohol on the morphology and anti-corrosion performance of phosphate coating applied on steel surface, J. Taiwan Inst. Chem. Eng. 58 (2016) 542–551.
[16] B. Ramezanzadeh, H. Vakili, R. Amini, The effects of addition of poly(vinyl) alcohol (PVA) as a green corrosion inhibitor to the phosphate conversion coating on the anticorrosion and adhesion properties of the epoxy coating on the steel substrate, Appl. Surf. Sci. 327 (2015) 174–181.
[17] S.S. Golru, M.M. Attar, B. Ramezanzadeh, Morphological analysis and corrosion performance of zirconium based conversion coating on the aluminum alloy 1050, J. Ind. Eng. Chem. 24 (2015) 233–244.
[18] S. Sharifi Golru, M.M. Attar, B. Ramezanzadeh, Effects of surface treatment of aluminium alloy 1050 on the adhesion and anticorrosion properties of the epoxy coating, Appl. Surf. Sci. 345 (2015) 360–368.
[19] S. Mu, J. Du, H. Jiang, W. Li, Composition analysis and corrosion performance of a Mo–Ce conversion coating on AZ91 magnesium alloy, Surf. Coat. Technol. 254 (2014) 364–370.
[20] R. Shoja Gharabagh, A. Sabour Rouhaghdam, Corrosion of environmentally friendly lanthanum conversion coating on AA2024-T3 aluminum alloy, Prot. Met. Phys. Chem 50 (2014) 88–93.

[21] M.G.S. Ferreira, R.G. Duarte, M.F. Montemor, A.M.P. Simões, Silanes and rare earth salts as chromate replacers for pre-treatments on galvanised steel, Electrochim. Acta 49 (2004) 2927–2935.
[22] M.F. Montemor, A.M. Simões, M.J. Carmezim, Characterization of rare-earth conversion films formed on the AZ31 magnesium alloy and its relation with corrosion protection, Appl. Surf. Sci. 253 (2007) 6922–6931.
[23] L. Hamlaoui, F. Tifouti, Corrosion behaviour of molybdate–phosphate–silicate coatings on galvanized steel, Corros. Sci. 51 (2009) 2455–2462.
[24] H.-Y. Su, C.-S. Lin, Effect of additives on the properties of phosphate conversion coating on electrogalvanized steel sheet, Corros. Sci. 83 (2014) 137–146.
[25] G. Kong, L. Lingyan, J. Lu, C. Che, Z. Zhong, Corrosion behavior of lanthanum-based conversion coating modified with citric acid on hot dip galvanized steel in aerated 1 M NaCl solution, Corros. Sci. 53 (2011) 1621–1626.
[26] A. Ghanbari, M.M. Attar, The effect of zirconium-based surface treatment on the cathodic disbonding resistance of epoxy coated mild steel, Appl. Surf. Sci. 316 (2014) 429–434.
[27] L. Lei, J. Shi, X. Wang, D. Liu, H. Xu, Microstructure and electrochemical behavior of cerium conversion coating modified with silane agent on magnesium substrates, Appl. Surf. Sci. 376 (2016) 161–171.
[28] E. Onofre-Bustamante, M.A. Domínguez-Crespo, A.M. Torres-Huerta, A. Olvera-Martínez, J. Genescá-Llongueras, F.J. Rodríguez-Gómez, Characterization of cerium-based conversion coatings for corrosion protection of AISI-1010 commercial carbon steel, J. Solid State Electrochem. 13 (2009) 1785–1799.
[29] Alessandro De Nicolò, Luca Paussa, Alice Gobessi, Alex Lanzutti, Lorenzo Fedrizzi, Cerium conversion coating and sol–gel multilayer system for corrosion protection of AA6060, Surf. Coat. Technol. 287 (2016) 33–43.
[30] G. Yoganandan, K. Pradeep Premkumar, J.N. Balaraju, Evaluation of corrosion resistance and self-healing behavior of zirconium–cerium conversion coating developed on AA2024 alloy, Surf. Coat. Technol. 270 (2015) 249–258.
[31] Jing Zhang, Xingye Guo, Yeon-Gil Jung, Li Li, James Knapp, Lanthanum zirconate based thermal barrier coatings: a review, Surf. Coat. Technol. 323 (2017) 18–29.
[32] Advanced microcapsules for self-healing conversion coating on magnesium alloy in Ce(NO3)3 solution with microcapsules containing La(NO3)3, Surf. Coat. Technol. 307 (2016) 500–505.
[33] Sina S. Jamali, Simon E. Moulton, Dennis E. Tallman, Yue Zhao, Gordon G. Wallace, Self-healing characteristic of praseodymium conversion coating on AZNd Mg alloy studied by scanning electrochemical microscopy, Electrochem. Commun. 76 (2017) 6–9.
[34] Sina S. Jamali, Simon E. Moulton, Dennis E. Tallman, Maria Forsyth, Gordon G. Wallace, Corrosion protection afforded by praseodymium conversion film on Mg alloy AZNd in simulated biological fluid studied by scanning electrochemical microscopy, J. Electroanal. Chem. 739 (2015) 211–217.
[35] Zhao Dingzang, Zhang Dingfei, Liu Yuping, Hu Guangshan, Pan Fusheng, Neodymium-based conversion coating on AZ31 magnesium alloy, Rare Met. Mater. Eng. 46 (2) (2017) 289–295.
[36] Xiufang Cui, Guo Jin, Yuyun Yang, Erbao Liu, Jinggao Zhong, The formation of neodymium conversion coating and the influence of post-treatment, Appl. Surf. Sci. 258 (7) (2012) 3249–3254.
[37] Z. Mahidashti, T. Shahrabi, B. Ramezanzadeh, A new strategy for improvement of the corrosion resistance of a green cerium conversion coating through thermal treatment procedure before and after application of epoxy coating, Appl. Surf. Sci. 390 (2016) 623–632.
[38] B. Ramezanzadeh, H. Vakili, R. Amini, Improved performance of cerium conversion coatings on steel with zinc phosphate post-treatment, J. Ind. Eng. Chem. 30 (2015) 225–233.
[39] T.G. Harvey, Cerium-based conversion coatings on aluminium alloys: a process review, Corrosion Engineering, Sci. Technol. 48 (2013) 248–269.
[40] Chao-Sung Lin, W.-J. Li, Corrosion resistance of cerium-Conversion coated AZ31 magnesium alloys in cerium nitrate solutions, Materi. Trans. 47 (2006) 1020–1025.
[41] D.K. Heller, W.G. Fahrenholtz, M.J. O'Keefe, The effect of post-treatment time and temperature on cerium-based conversion coatings on Al 2024-T3, Corros. Sci. 52 (2010) 360–368.
[42] Hossein Hassannejad, Mohsen Moghaddasi, Ehsan Saebnoori, Amin Rabiein Baboukani, Microstructure, deposition mechanism and corrosion behavior of nanostructured cerium oxide conversion coating modified with chitosan on AA2024 aluminum alloy, J. Alloys Compd. 725 (2017) 968–975.
[43] Li Lei, Jing Shi, Xin Wang, Dan Liu, Haigang Xu, Microstructure and electrochemical behavior of cerium conversion coating modified with silane agent on magnesium substrates, Appl. Surf. Sci. 376 (2016) 161–171.
[44] A.P. Loperena, I.L. Lehr, S.B. Saidman, Formation of a cerium conversion coating on magnesium alloy using ascorbic acid as additive. Characterization and anticorrosive properties of the formed films, J. Magnesium Alloys 4 (4) (2016) 278–285.
[45] G. Yoganandan, K. Pradeep Premkumar, J.N. Balaraju, Evaluation of corrosion resistance and self-healing behavior of zirconium–cerium conversion coating developed on AA2024 alloy, Surf. Coat. Technol. 270 (2015) 249–258.
[46] Nguyen Van Phuong, Manoj Gupta, Sungmo Moon, Adhesion and corrosion studies of electrophoretic paint on AZ31 Mg alloy pretreated in cerium solution with and without addition of ethanol, Prog. Org. Coat. 102 (2017) 144–150.
[47] S. Živković, B.V. Jegdić, J.P. Popić, J.B. Bajat, V.B. Mišković-Stanković, The influence of Ce-based coatings as pretreatments on corrosion stability of top powder polyester coating on AA6060, Prog. Org. Coat. 76 (10) (2013) 1387–1395.
[48] Ljiljana S. Živković, Jelena B. Bajat, Jovan P. Popić, Bore V. Jegdić, Vesna B. Mišković-Stanković, Protective properties of cataphoretic epoxy coating on aluminium alloy AA6060 modified with electrodeposited Ce-based coatings: effect of post-treatment, Prog. Org. Coat. 79 (2015) 43–52.
[49] M. Golabadi, M. Aliofkhazraei, M. Toorani, A. Sabour Rouhaghdam, Evaluation of La containing PEO pretreatment on protective performance of epoxy coating on magnesium, Prog. Org. Coat. 105 (2017) 258–266.
[50] A.Y. El-Etre, Khillah extract as inhibitor for acid corrosion of SX 316 steel, Appl. Surf. Sci. 252 (2006) 8521–8525.
[51] D. Chadwick, T. Hashemi, Adsorbed corrosion inhibitors studied by electron spectroscopy: benzotriazole on copper and copper alloys, Corros. Sci. 18 (1978) 39–51.
[52] B.E.A. Rani, B.B.J. Basu, Green inhibitors for corrosion protection of metals and alloys: an overview, Int. J. Corros. 2012 (2012).
[53] M. Jokar, T.S. Farahani, B. Ramezanzadeh, Electrochemical and surface characterizations of morus alba pendula leaves extract (MAPLE) as a green corrosion inhibitor for steel in 1 M HCl, Journal of the Taiwan Institute of Chemical Engineers 63 (2016) 436–452.
[54] A. Ostovari, S.M. Hoseinieh, M. Peikari, S.R. Shadizadeh, S.J. Hashemi, Corrosion inhibition of mild steel in 1 M HCl solution by henna extract: a comparative study of the inhibition by henna and its constituents (Lawsone, Gallic acid, α-d-Glucose and Tannic acid), Corros. Sci. 51 (2009) 1935–1949.
[55] M. Nasibi, E. Mohammady, A. Ghasemi, D. Ashrafi, G. Zaarei, Corrosion inhibition of mild steel by Nettle (Urtica dioica L.) extract: polarization, EIS, AFM, SEM and EDS studies, J. Adhes. Sci. Technol. 27 (2013) 1873–1885.
[56] Z. Aida, A. Razika, M. Laid, B. Kamel, S. Boualem, Inhibition of acid corrosion of mild steel by aqueous nettle extracts, Pigment Resin Technol. 43 (2014) 127–138.
[57] A. Fattah-alhosseini, B. Hamrahi, Corrosion inhibition of API 5L carbon steel by nettle leaves hydroalcoholic extract in a 0.5 M H2SO4 solution, Int. J. Iron Steel Soc. Iran 13 (2016) 45–49.
[58] D. Orčić, M. Francišković, K. Bekvalac, E. Svirčev, I. Beara, M. Lesjak, N. Mimica-Dukić, Quantitative determination of plant phenolics in Urtica dioica extracts by high-performance liquid chromatography coupled with tandem mass spectrometric detection, Food Chem. 143 (2014) 48–53.
[59] S. Otles, B. Yalcin, Phenolic compounds analysis of root stalk, and leaves of nettle, Sci. World J. 2012 (2012) 564367.
[60] N. Issaoui, H. Ghalla, F. Bardak, M. Karabacak, N. Aouled Dlala, H.T. Flakus, B. Oujia, Combined experimental and theoretical studies on the molecular structures, spectroscopy, and inhibitor activity of 3-(2-thienyl)acrylic acid through AIM, NBO,FT-IR, FT-Raman, UV and HOMO-LUMO analyses, and molecular docking, Journal of Molecular Structure 1130 (2017) 659–668.
[61] A.Y. El-Etre, A.I. Ali, A Novel Green Inhibitor for C- Steel Corrosion in 2. 0 Mol·L- 1 Hydrochloric Acid Solution, Chinese Journal of Chemical Engineering 25 (3) (2017) 373–380.
[62] J.E. Stewart, Vibrational spectra of primary and secondary aliphatic amines, J. Chem. Phys. 30 (1959) 1259–1265.
[63] E. Günister, D. Pestreli, C.H. Ünlü, O. Atıcı, N. Güngör, Synthesis and characterization of chitosan-MMT biocomposite systems, Carbohydr. Polym. 67 (2007) 358–365.
[64] S.M. Hoseinieh, A.M. Homborg, T. Shahrabi, J.M.C. Mol, B. Ramezanzadeh, A novel approach for the evaluation of under deposit corrosion in marine environments using combined analysis by electrochemical impedance spectroscopy and electrochemical noise, Electrochim. Acta 217 (2016) 226–241.
[65] D.E. Arthur, A. Jonathan, P.O. Ameh, C. Anya, A review on the assessment of polymeric materials used as corrosion inhibitor of metals and alloys, Int. J. Ind. Chem. 4 (2013) 1–9.
[66] J.J. Bikerman, The Science of Adhesive Joints, Academic Press, New York, 1968.
[67] N.J. Delollis, O. Montaya, Mode of failure in structural adhesive bonds, J. Appl. Polym. Sci. 11 (1967) 983–989.
[68] R.A. Dickie, F.L. Floyd, Polymeric materials for corrosion control: an overview, in: polymeric materials for corrosion control, Am. Chem. Soc. (1986) 1–16.
[69] Ghasem Bahlakeh, Bahram Ramezanzadeh, A detailed molecular dynamics simulation and experimental investigation on the interfacial bonding mechanism of an epoxy adhesive on carbon steel sheets decorated with a novel cerium-Lanthanum nanofilm, ACS Appl. Mater. Interfaces 9 (2017) 17536–17551.
[70] E. Salehi, R. Naderi, B. Ramezanzadeh, Synthesis and characterization of an effective organic/inorganic hybrid green corrosion inhibitive complex based on zinc acetate/Urtica Dioica, Appl. Surf. Sci. 396 (2017) 1499–1514.